STRUCTURAL, ELECTRONIC, OPTICAL, AND THERMOELECTRIC PROPERTIES OF β PHASE SPINEL: PROSPECTS FOR SOLAR CELLS APPLICATION

L. MOHAMMED[a,b], A. R. MAT ISA[a], A. MUSA[a], TARIQ MAHMOOD[c], M. A. SAEED[a*]
[a]*Department of Physics, Faculty of Science, Universiti Teknologi Malaysia, 81310 UTM Johor Bahru, Johor, Malaysia*
[b]*Department of Physics, Faculty of Science, Ahmadu Bello University, Zaria, 833201, Zaria, Kaduna, Nigeria*
[c]*Centre for Excellence Solid State Physics, University of the Punjab, Lahore-54590, Pakistan*

Using all electron based density functional theory calculations, within full potential linearized augmented plane wave plus local orbitals, electronic, structural, optical and thermoelectric properties of the β-phase spinel compound have been investigated. Tetragonal β-phase spinel indium (III) sulfide is the most stable and promising phase for various applications, in particular, photovoltaic devices, and, therefore, it can be use to replace CdS for environmental issues. The unit cell volume and atomic positions are optimized with the PBE energy functional and our calculated optical band gap for the indirect transition is in good agreement with the experimental value. The peaks of the real part of optical conductivity $\sigma(\omega)$ correspond to the peak of the imaginary part of dielectric function $\varepsilon_i(\omega)$ for the two polarization axes, which perfectly agree with the Drude theory. Charge carrier concentration are observed to attain the maximum value at about 2.8899 eV at fixed temperature, and drops at high energies, which indicates less photon excitation to the conduction bands at energies greater than 2.8899 eV. The electrical and thermal conductivity that depends on the sulfur concentration show a similar trend for variable and fixed temperature. Large amount of thermopower *S* occurs at low temperature, which agrees with the requirement to improve performance of photovoltaic materials, that is high voltage output at small amount of heat.

(Received November 16, 2015; Accepted January 4, 2016)

Keywords: Electronic; Seebeck coefficient; Fermi surface; Solar cell; Optical properties

1. Introduction

Spinel indium sulfide (In_2S_3) exists in three phases. The tetragonal β-phase transforms to the cubic α-phase at 420 ^oC, which further transforms to the γ-phase at 750 ^oC. Due to wide energy bandgap, the phases of indium sulfide have possibilities of applications in photo-electrochemical solar cells devices [1]. However, the β-phase Indium sulphide is the only stable crystallized spinel among the existing three phases that shows potential photovoltaic properties [2-4], It is used as an absorber material [5], and as buffer layer in C-In-Ga-S (CIGS) based thin film solar cells, due to its exceptional photoelectric properties [6].

The β-In_2S_3 ($In_{16}S_{24}$ primitive unit cell) crystal lattice can be considered as a defect structure of the $MgIn_4S_8$ spinel with Mg vacancies and with a ¼ of Indiums at tetrahedral sites and

*Corresponding author: saeed@utm.my

the rest at the octahedral ones. Furthermore, the β-phase has a defect spinel structure with indium vacancies ordered in the tetrahedral sites with space group: $I4_1/amd$. The In atoms located at three different lattice positions, In1(8c), In2(16h), and In3(8e), and thus there are three kinds of In-S polyhedral structures. The In1-S and In2-S have distorted octahedrons, which linked with each other by a shared edge. This defect slightly affects the properties of this compound [2]. The electrical and optical properties of beta phase In_2S_3 are stable at normal temperature. It has energy band gap ranging from 1.90 eV to 2.10 eV [7]. Another interest in this compound arises in the study of defect engineering [8], and in intermediate band material [9-12] for the high efficiency solar cell as buffers [1, 13]. Chemical salvo-thermal methods have been used to successfully synthesize $V_{0.25}In_{1.75}S_3$ that has strong sub-bandgap absorption and an inherent partially filled intermediate band [14]. Moreover, it also has potential applications in the preparation of green and red phosphors, in the manufacture of picture tubes for color television, and in infrared optical technology [15]. It also has application in various aspect of thin film technology [16-18], in which optical spectroscopy analysis was used to tune the annealing condition for transmittance study.

The present work is an attempt to study the ground state and transport properties of β-ln_2S_3 ($ln_{16}S_{24}$ primitive unit cell), by using one of the most accurate all electron density functional theory and Boltztrap code respectively. Therefore, structural, electronic, optical, and thermoelectric properties are calculated and analyzed based on it suitability for the photovoltaic application.

2. Methodology

We have carried out detail study of structural, electronic, and optical properties using density functional theory [19], within full potential linearized augmented plane wave plus local orbitals (FP-LAPW+lo) as implemented in one of the most accurate methods in WIEN2K code [20]. The exchange correlation potential is treated using the generalized gradient approximation [21]. In this approach, the unit cell is partitioned into non-overlapping muffin-tin spheres around the atomic sites and an interstitial region. In these two types of region, different basis sets are used inside the atomic sphere (t) of radius (R_t), the other inside the interstitial region. In this scheme, the basis set is energy independent, and possesses two functions augmented to obtain a good description of the wave functions. Tetrahedron method of integration is used on a grid of 159 k-point in the irreducible Brillouin zone, which gives the minimum ground state energy, as depicted in Figure 1(c). This value is far better than -207,392.42 eV [3], this could be due denser mesh used in this calculation. For optimum accuracy we set $R_{MT}K_{max} = 8, and\ l_{max} = 10$, these are energy cut-off of the plane wave expansion and upper limit of the angular momentum expansions of the wave functions inside the non-overlapping spheres surrounding the atomic sites respectively. The matrix size and local orbital used are 6,896 and 408 respectively. Here, we have used X-ray diffraction experiment data to generate Crystallographic Information File to use for this study [22]. Table 1 shows the precise lattice vectors of the tetragonal body centered β-In2S3 structure and the general position vectors of the space Group 141/amd in the given setting (0, 0, 0), (1/2, 1/2, 1/2). Both optical and transport properties are calculated using Kramers-Kronig relation [23], and semi-classical Boltzmann transport equation, [24]. In transport equation the electronic thermal conductivity, k_{el}, at zero electrical current is defined as:

$$k_{el} = k^0 - T\sigma S^2 \tag{1}$$

Where k^0 is given by

$$k^0_{\alpha\beta}(T;\mu) = \frac{1}{e^2T\Omega}\int \sigma_{\alpha\beta}(\varepsilon)(\varepsilon-\mu)^2\left\{-\frac{\partial f_\mu(T,\varepsilon)}{\partial\varepsilon}\right\}d\varepsilon \tag{2}$$

Where T is the temperature, σ electrical conductivity, S the Seebeck coefficient, assuming the electronic thermal conductivity is independent of the relaxation time τ. The carrier concentration n, thermopower S, electrical and electronic thermal conductivity at fixed and variable temperature is calculated.

3. Results and discussion

3.1 Structural and Electronic Properties

The crystal structure of β-In_2S_3 is optimized, the lowest ground state energy and the corresponding volumes of unit cell that agree with experimental values are determined as shown in Figure 1(a and b). This was achieved by using energy versus volume curve fitted to the Birch-Murnaghan equation of state [25]. Our calculated volume of the optimized unit cell is 1875.89 A^3 which is in good agreement with the experimental values of 1875.86 A^3 [15]. This infers that our method and the results are good. The relaxed structure is obtained when the variations in energies with the change in c/a ratio is calculated and plotted as in Figure 1(b). This is further used for all the calculations.

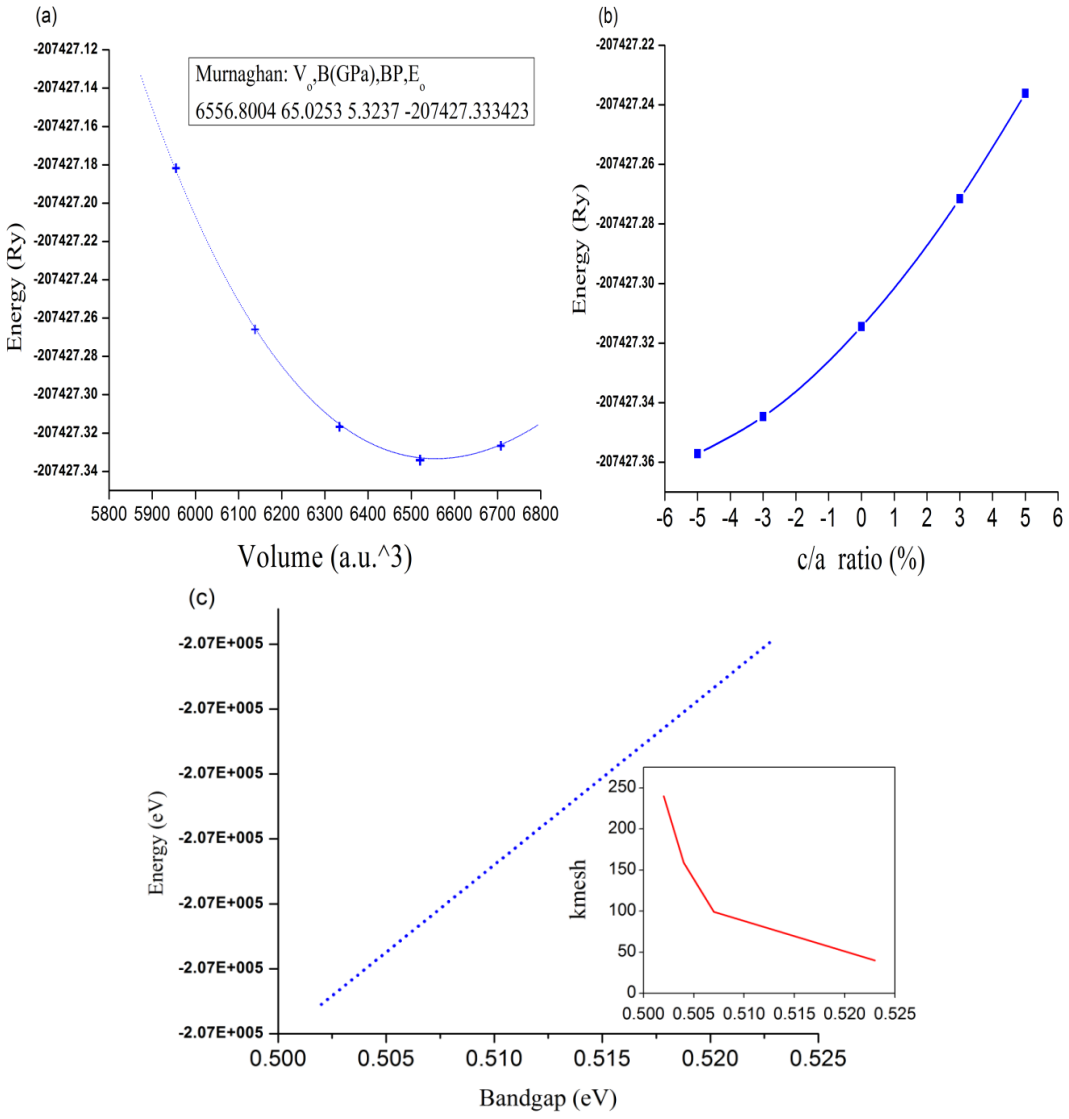

Fig. 1 (a) the optimized volume curve as a total energy versus unit cell volume of the β-In_2S_3 crystal within GGA (b) variation of total energy versus c/a ratio (c) Band gap as a function of ground state energy. The inset shows the corresponding kmesh in the irreducible Brillouin zone.

Table 1 Position vector and General Positions of the Space Group of the β-In_2S_3

Position vector	General Positions of the Space Group
x,y,z	x,y,z
x+1/2,y+1/2,z+1/2	-x+1/2,-y,z+1/2
x,-y,-z	-y+1/4,x+3/4,z+1/4
x+1/2,-y+1/2,-z+1/2	y+1/4,-x+1/4,z+3/4
-x,y+1/2,-z	-x+1/2,y,-z+1/2
-x+1/2,y,-z+1/2	x,-y,-z
-x,-y+1/2,z	y+1/4,x+3/4,-z+1/4
-x+1/2,-y,z+1/2	-y+1/4,-x+1/4,-z+3/4
-y+1/4,-x+1/4,-z+3/4	-x,-y,-z
-y+3/4,-x+3/4,-z+1/4	x+1/2,y,-z+1/2
-y+1/4,x+3/4,z+1/4	y+3/4,-x+1/4,-z+3/4
-y+3/4,x+1/4,z+3/4	-y+3/4,x+3/4,-z+1/4
y+3/4,-x+3/4,z+1/4	x+1/2,-y,z+1/2
y+1/4,-x+1/4,z+3/4	-x,y,z
y+3/4,x+1/4,-z+3/4	-y+3/4,-x+1/4,z+3/4
y+1/4,x+3/4,-z+1/4	y+3/4,x+3/4,z+1/4
-x,-y,-z	x,y,z
-x+1/2,-y+1/2,-z+1/2	-x+1/2,-y,z+1/2
-x,y,z	-y+1/4,x+3/4,z+1/4
-x+1/2,y+1/2,z+1/2	y+1/4,-x+1/4,z+3/4
x,-y+1/2,z	-x+1/2,y,-z+1/2
x+1/2,-y,z+1/2	x,-y,-z
x,y+1/2,-z	y+1/4,x+3/4,-z+1/4
x+1/2,y,-z+1/2	-y+1/4,-x+1/4,-z+3/4
y+3/4,x+3/4,z+1/4	-x,-y,-z
y+1/4,x+1/4,z+3/4	x+1/2,y,-z+1/2
y+3/4,-x+1/4,-z+3/4	
y+1/4,-x+3/4,-z+1/4	
-y+1/4,x+1/4,-z+3/4	
-y+3/4,x+3/4,-z+1/4	
-y+1/4,-x+3/4,z+1/4	

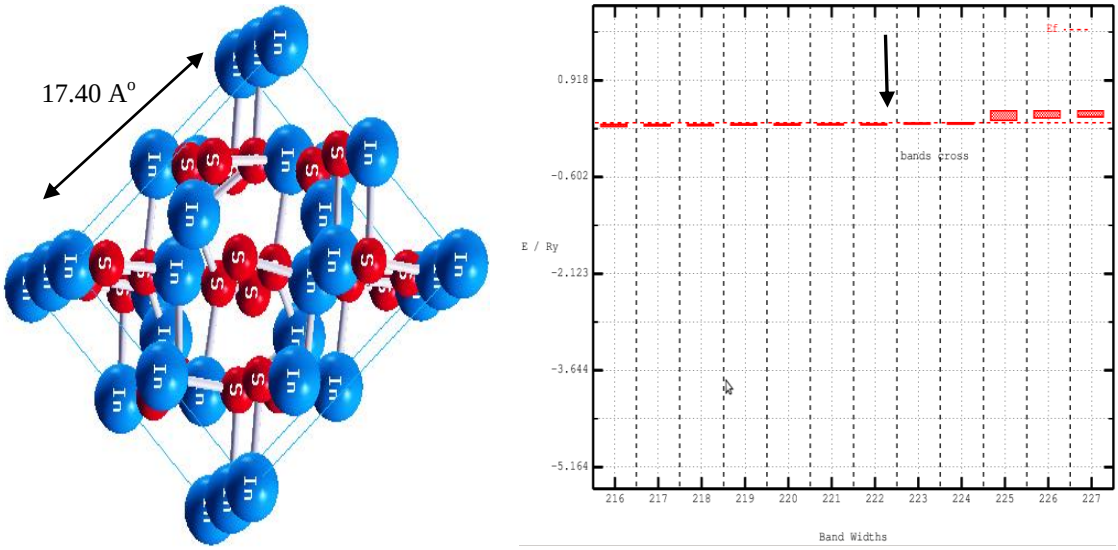

Fig. 2 (a) Primitive unit cell of body centered β-In_2S_3 structure (b) BAR Graph showing the band widths and bands that intersect the Fermi level.

The lowest ground state energy obtained for GGA energy functional is about -2.8 MeV. However, the ground state energy is shown to vary with energy gap and mesh of k-point inside the irreducible BZ as shown in (Figure 1(c)), band gap increases with the rise of k-points. A bandgap of about 1.523 eV is observed for the lowest mesh of 500, which is reasonable due to the band gap underestimation by GGA functional. In Figure 2(a), a primitive unit cell of the tetragonal body centered β-In_2S_3 crystal with two sets of 2.68 A^o and 2.60 A^o as coordination between Indium and Sulfur atoms agrees with experiment [15]. The energy level density for two dimensional Fermi surface is plotted using Wien2K package as shown in Figure 3(a). This was achieved by using BARGraph (Figure 2(b)) created with xcrysden [26] to identify bands that cross the Fermi level. These bands are 216 to 224 (as pointed by the arrow) out of 485 total bands.

3.2 Optical and Thermoelectric Properties

The compounds with tetragonal symmetry have two non-zero components of the dielectric tensor. Real $\varepsilon_r(\omega)$ and imaginary $\varepsilon_i(\omega)$ dielectric functions help in understanding the optical behavior of the material; these are plotted, together with optical absorption and conductivity as a function of frequency in Figure 3(b). The peaks from $\varepsilon_i(\omega)$ occur at 5.087 eV for E_{xx} and 6.276 eV for E_{zz} this indicates considerable anisotropy between the two spectra corresponding to the different polarization of this compound. Furthermore, this phase shows birefringence stronger than some reported solar cell material [27], which means that it refractive index depends on the polarization and propagation direction of light. Hence, β-In_2S_3 is an anisotropic material.

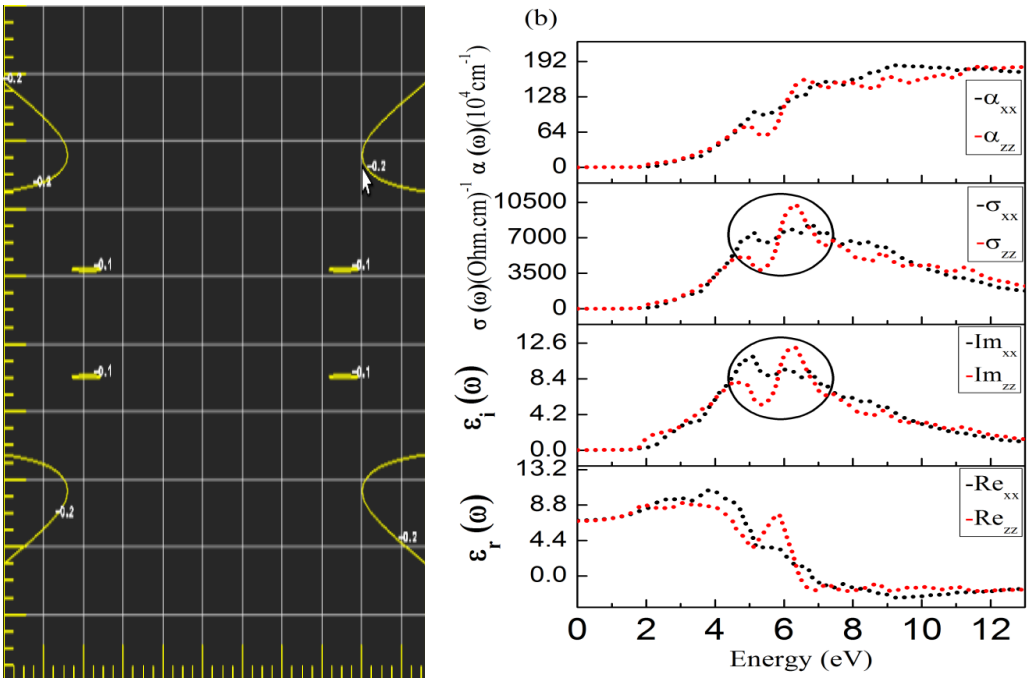

Fig. 3 (a) Left calculated 2D Fermi surface with energy label density (b) from bottom to top calculated real dielectric function $\varepsilon_r(\omega)$ imaginary dielectric function $\varepsilon_i(\omega)$ real part of optical conductivity $\sigma(\omega)$ and absorption coefficient $\alpha(\omega)$.

Static dielectric constants at zero frequency are nearly same for the two polarization axes. It is about 6.85 and the index of refraction is about 1.85 as calculated using $n(\omega) = \frac{(\varepsilon_1 + (\varepsilon_1^2 + \varepsilon_2^2)^{1/2})^{1/2}}{\sqrt{2}}$. The absorption coefficient and optical conductivity is shown in Figure 3(b)). The two plots show similar trend for both polarization axes, so that, high absorption and optical conductivity occur at about 6.32 eV and 6.54 eV for E_{zz} respectively. The peaks of the real part of the optical conductivity $\sigma(\omega)$ correspond to the peak of the imaginary part of dielectric function for the two polarization axes. These peaks are known as the Drude peaks, the width of the

peaks is equal to the inverse relaxation time of electrons. According to Drude theory, the real part of optical conductivity and the imaginary part of dielectric function has a peak at low frequency. For the *x*-polarization axis, this peak occurs at about 5.07 eV as highlighted by the circle in figure 3(b). Another way of predicting electrical, optical, and thermal properties of crystal is by analyzing the periodicity and symmetry of crystalline lattice derived from Fermi surface and occupation of electronic energy bands. Figure 3(a) shows 2D Fermi surface plotted in reciprocal space with energy label density, the solid lines represent the Fermi surfaces.

The calculated absorption coefficients is in agreement with the experimental ones [14]. The absorption spectra rise steeply at the absorption edge; peaks are observed to be around 5.20 eV, and 6.63 eV for the *xx*, and *zz* polarization directions respectively. There is a steady increase within the visible range of the solar spectrum, and becomes high at the violet part of the wavelength.

The optical band gap shown in Figure 4 is far greater than the band gap; this might be because the absorption at the gap edge is forbidden due to the matrix element $\langle vk|p_i|ck\rangle\langle ck|p_j|vk\rangle$, which determines the probability of electron jumping between the single particle states. It produces oscillation and renders absorption possible when these matrices are zero. The β-In_2S_3 possess direct and indirect electronic transition, as such both direct and indirect optical energy gaps are calculated as shown in Figure 4(a and b). The direct and indirect optical energy band gap is calculated by using the relation $(\alpha hvn)^n = A\left(hv - E_g\right)$, where *hv* is the incident photon energy and α is the, optical absorption coefficient calculated near the fundamental absorption edge. The value of $(\alpha hvn)^n$ (where n=2 or ½ for direct and indirect optical energy gap respectively) is plotted as a function of incident photon energy (*hv*) as shown in Figure 4(a and b). Our calculated direct optical gap is about 3.395 eV, the experimental one is 2.639 eV, while the indirect optical gap is 2.265eV and the experiment is 2.240 eV [28]. This shows a good agreement with the experiment, but the discrepancy between direct optical gaps with the experiment may be due to high quantum efficiency of direct transition for the emission of light.

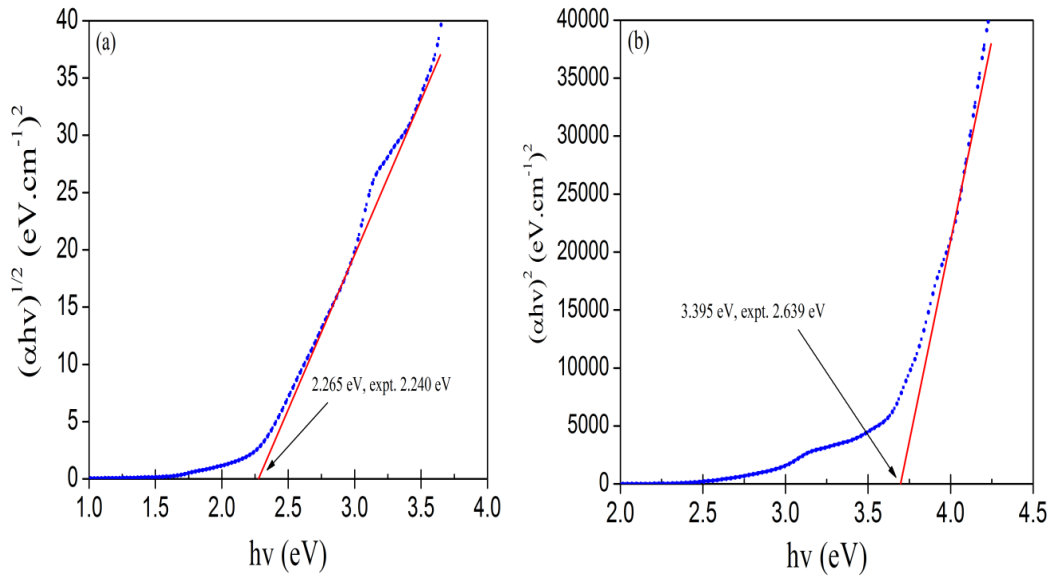

Fig 4 (a) Plot of the linear part of the absorbance spectrum for indirect optical energy band gap (b) linear part of the absorbance spectrum for direct optical energy band gap

Figure 5(a and b), show the calculated thermoelectric parameters, carrier concentration *n*, thermopower *S*, electrical and thermal conductivity at 420 K and variable temperature. Charge carrier concentration as a function of chemical potential μ attains its maximum value at about 3.0 eV for fixed temperature, and it drops at high energies. This indicates low photon excitation to the conduction bands at energies > 3.0 eV. This would not be a problem since the maximum reported energy gap for this compound is < 2.8899 eV [28]. At very low value of μ carrier concentration is

about 984 *e/uc*, which implies that β-In_2S_3 crystal cannot have insulating properties at 420 K. Similar trend is observed in figure 5(b), in which the peak for the carrier concentration as a function of temperature occurs at about 240 K. Both electrical and thermal conductivity depends on the sulfur concentration [1], showing a similar trend for variable and fixed temperature. However, a gradual decrease in the two values of conductivities as it approaches 2.8899 eV is observed and rises steadily at higher energies.

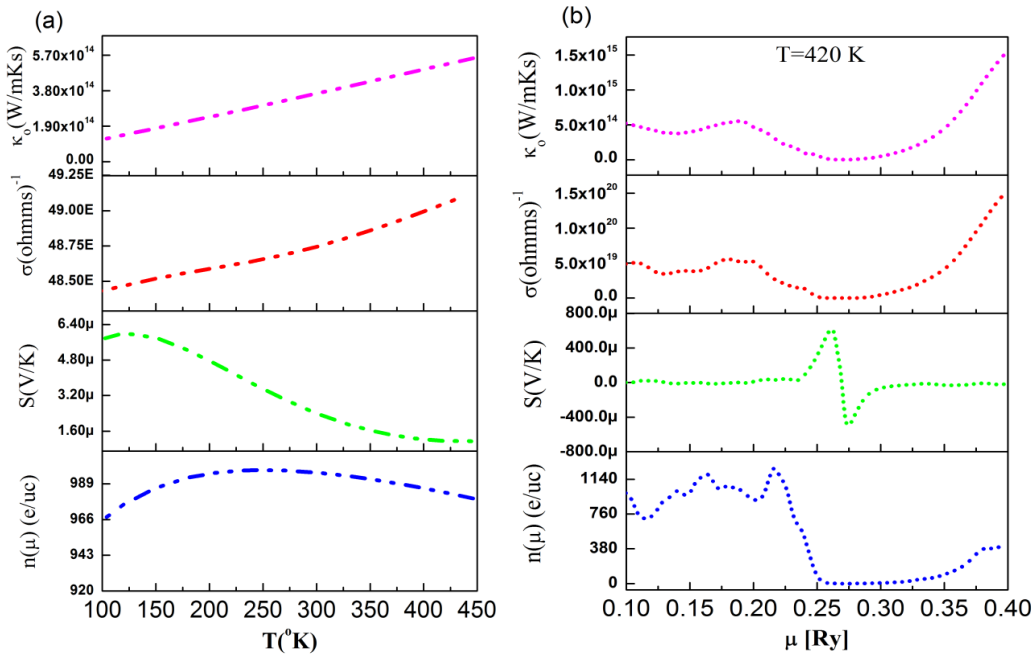

Fig. 5. (a) Calculated thermoelectric properties, n, S, σ, κ_o as function of temperature variation (b) thermoelectric properties n, S, σ, κ_o at constant temperature

However, the thermal conductivity κ_o has no appreciable responses at low temperature, whereas, at the lowest value of chemical potential κ_o is observed to be greater than the low temperature case. Thermoelectric voltage is induced due to the temperature difference in material. Higher thermoelectric voltage for a given temperature gradient may lead to improve efficiency because high Seebeck coefficient is required to convert the maximum heat to electrical power. Ideally, large thermopower is required since only a small amount of heat is needed to produce a large voltage. This situation is depicted in (Figure 5(a)) in which the highest Seebeck coefficient about 6.0 μV K^{-1} occurs at low temperature. This further confirms the stability of the beta phase Indium sulfide as solar cell material.

4. Conclusion

In summary, this paper presents a detailed study of the β-phase Indium sulfide with reference to solar energy conversion properties. It is shown that when the temperature is varied, high thermopower might be achieved at reasonably low energy, which may enhance heat to electric power conversion. The results show that variation of $\alpha h\nu$ as a function of photon energy for indirect transition is in good comparison with the experimental results.

Acknowledgements

The authors thank the Ahmadu Bello University Zaria-Nigeria, for support and study fellowship to M. Lawal through Tertiary institutions Educational Trust Fund (TETFUND).

The authors would like to thank for the financial support by the Ministry of Higher Education (MOHE) Malaysia and Universiti Teknologi Malaysia (UTM) under Grant No Q.J130000.2526.06H14.

References

[1] N. Barreau, Solar Energy. 83 (2009) 363-371.
[2] Z. Zhao, J. Yi, D. Zhou, Computational Materials Science. 73 (2013) 139-145.
[3] Y. Sharma, Srivastava, Pankaj, Materials Chemistry and Physics. 135 (2012) 385-394.
[4] S. Marsillac, N.S. Mangale, V. Gade, S.V. Khare, Thin Solid Films. 519 (2011) 5679-5683.
[5] T.T.J. R. Jayakrishnan, C.S. Kartha, K.P. Vijayakumar, D. Jain, L.S. Chandra, V. Ganesan, J. Appl. Phys. 053106. 103 (2008) 053106.
[6] H.C.H. W. Yi Ping, H. Ying Sheng, , J. Phys. D. Appl. Phys. . 43 (2010) 415301.
[7] N.B. J.C. Berne`De, S. Marsillac, L. Assmann, Applied Surface Science. 195 (2002) 222–228.
[8] X.R. A. Lafond, M. Paris, C. Guillot-Deudon, and V. Jouenne, Chem. Mater.2011, 23, 23 (2011) 9.
[9] C.-H. Ho, J. Mater. Chem. 21 (2011) 6.
[10] I.A. P.Wahnón, P.Palacios, K.Sánchez, and J.C.Conesa, (2009) 4.
[11] P. Palacios, I. Aguilera, K. Sánchez, J. Conesa, P. Wahnón, Physical Review Letters. 101 (2008).
[12] P. Chen, H. Chen, M. Qin, C. Yang, W. Zhao, Y. Liu, W. Zhang, F. Huang, Journal of Applied Physics. 113 (2013).
[13] N. Barreau, J.C. Bernède, S. Marsillac, C. Amory, W.N. Shafarman, Thin Solid Films. 431-432 (2003) 326-329.
[14] L. Antonio, Antonio, Martí, and Colin, Stanley, Nature Photonics. 6 (2012) 146-152.
[15] A.M.V. Niyum S. Rampersadh, David G. Billing, Physica B 350. 350 (2004) 3.
[16] M.L.a.H. Ezzaouia, The Open Applied Physics Journal. 2 (2009) 4.
[17] B.a.K. M.M. El-Nahassa, H.S. Soliman, M.A.M. Seyam, Thin Solid Films 515 (2006). 515 (2006) 6.
[18] M.K.J. Rahana Yoosuf, Solar Energy Materials & Solar Cells. 89 (2005) 10.
[19] J.a.S. David S. Sholl, Published by John Wiley & Sons, Inc., Hoboken, New Jersey. (2009).
[20] K.S. Peter Blaha, Georg K. H. Madsen, Dieter Kvasnicka, Joachim Luitz, (2014) 258.
[21] J.P. Perdew, Burke S, Ernzerhof, M., Phys Rev Lett. 77 (1996) 3865-86.
[22] J.M.P.-M. M. I. Aroyo, C. Capillas, E. Kroumova, S. Ivantchev, G. Madariaga, A. Kirov & H. Wondratschek, Crystalline Materials. 221 (2006) 15-27.
[23] P. Puschnig C. Ambrosch-Draxl, Advanced Engineering Materials. 8 (2006) 1151-1155.
[24] G.K.H. Madsen D.J. Singh, Computer Physics Communications. 175 (2006) 67-71.
[25] F. Birch, Physical Review. 71 (1947) 809-824.
[26] A. Kokalj, Computational Materials Science. 28 (2003) 155-168.
[27] T. Ben Nasr, Maghraoui-Meherzi, H., Ben Abdallah, H., Bennaceur, R., Physica B: Condensed Matter. 406 (2011) 287-292.
[28] T.-H.B. Sung-Hyu Choe, Nam-Oh Kim, Hyung-Gon Kim, Choong-Il Lee, Moon-Seog Jin, Seok-Kyun Oh and Wha-Tek Kim, Semicond. Sci. Technol. 16 (2001) 4.